JOURNAL OF THEORETICAL
AND APPLIED MECHANICS
64, 2, pp. 101–114, Warsaw 2026
https://doi.org/10.15632/jtam-pl/218270

RESEARCH ON THE PENETRATION RESISTANCE PERFORMANCE OF A CERAMIC BALL/NYLON ELASTOMER COMPOSITE STRUCTURE

Chaoming SHEN[1*], Shuming ZHAO[1], Kun TAN[2], Longqiang LI[1], Fushan LI[3], Tingwei WANG[3]

[1] *School of Naval Architecture and Ocean Engineering, Jiangsu University of Science and Technology, Zhenjiang, China*
[2] *Nanjing Traffic Comprehensive Administrative Law Enforcement Corps, Nanjing, China*
[3] *China Special Equipment Inspection and Research Institute, Jiaxing, China*

[*]corresponding author, *shencm@just.edu.cn*

This paper proposes a ceramic ball/nylon elastomer composite structure. Experimental testing and finite element analysis were conducted to investigate the influence of key factors on the penetration resistance of the composite structures with constant total thickness. These factors include ceramic ball diameter, arrangement pattern, projectile head configuration, and the ratio of projectile diameter to ceramic ball diameter. The results indicate that the composite structures with three configurations exhibit higher resistance to round-nose projectiles compared to flat-nose projectiles. For projectiles with a diameter of 8.08 mm (both round-nose and flat-nose), the composite structures with two-different-diameters ceramic balls exhibit better penetration resistance compared to those with single-diameter or triple-different-diameters ceramic balls. Furthermore, when the diameter ratio of the projectile to the front-layer ceramic balls falls within 0.73–1.01, the penetration resistance performance of the composite structure is relatively better, and optimal penetration resistance is achieved when the diameter ratio between the front-layer ceramic balls and other back-layer ceramic balls is 1.7–2.0. These findings provide valuable references for designing penetration-resistant protective structures for ships and other marine constructions.

Keywords: ceramic ball; composite structure; penetration resistance performance; residual velocity.

1. Introduction

In recent decades, maritime transportation has become one of the most important modes of global trade and energy supply. Naval and commercial vessels operating in high-risk environments may be exposed to ballistic impacts and explosive fragmentation, posing significant threats to personnel and onboard high-value equipment. Therefore, improving the penetration resistance of ship structures is essential for enhancing operational safety and survivability. Ceramic materials have been widely investigated for protective applications due to their high strength, high hardness, and light weight.

Research on ceramic composite protective structures dates back to the late 20th century. Early studies of Woodward (1990) revealed that upon projectile impact, a protective ceramic cone forms, which helps reduce the shock on the backing plate. Subsequently, Zaera *et al.* (2000) further clarified this mechanism, finding that thicker ceramic plates result in smaller cones and lower stress on the backing plate. Lee and Yoo (2001) discovered that for a fixed areal density, an optimal ceramic-to-metal thickness ratio existed that maximized penetration resistance. More recently, Cao *et al.* (2020) highlighted the significant influence of boundary constraints on ceramic performance, considering crack initiation and wear. In addition, Tan *et al.* (2021) found that

protective performance was optimized when the ceramic ball to projectile diameter ratio fell within a specific range. Feng and Zhu (2024) proposed a novel bionic composite with a rigid-flexible coupling structure, where soft and hard layers worked synergistically to dissipate impact energy through a progressive damage process.

In numerical analysis of penetration processes, Schwer and Day (1991) enhanced simulation accuracy by improving constitutive equations and optimizing meshes for armor-piercing projectiles and earth penetrators. Beissel and Johnson (2000) introduced the concept of an attrition surface to analyze real-time projectile damage and adjusted parameters to better simulate the penetration process. Fawaz *et al.* (2004) investigated the effect of incidence angles on ceramic–metal structures, finding that while kinetic energy remained similar, interlayer forces increased during full penetration. Feli and Asgari (2011) observed that ceramic cone angles increased with projectile velocity. Andraskar *et al.* (2023) concluded that the B4C ceramic plate had the best penetration resistance at a thickness of 7.5 mm. Aktaş and Çevik (2025) designed novel geometries of alumina ceramics, overcoming brittleness through spherical and triangular prism geometries. Additionally, Tan *et al.* (2023) developed a three-layer ceramic armor model, showing that layer sequence had little effect on ceramic damage compared to thickness. Existing research results show that the protective properties of ceramic composite structures are determined by the combination of material compatibility, geometric configuration and impact parameters: when impacted, the ceramic layer dissipates the kinetic energy of the projectile through crushing, while the backplate absorbs the remaining kinetic energy through deformation. Despite these advances, the multi-field coupling mechanisms governing energy transfer and failure evolution in complex protective structures remain insufficiently understood.

On the basis of the existing research, this paper proposes a ceramic ball/nylon elastomer composite protective structure, and through experiments and numerical simulations reveals the influence of structural parameters on its anti-elasticity performance, which can provide new ideas and references for the design of anti-penetration structures of marine vessels.

2. Numerical simulation methods

2.1. Establishment of numerical model

To investigate the influence of ceramic ball diameter and configuration on the penetration resistance of ceramic ball/nylon elastomer composite structures, numerical models of single-diameter, double-diameter and triple-diameter ceramic ball combination protection structures were developed, as shown in Fig. 1 and Fig. 2. The target plate has overall dimensions of 200 mm × 200 mm × 50 mm, with a 0.5 mm-thick steel plate on both its front and rear surfaces to form a sandwich structure. All target plates maintain a thickness of 50 mm, with internal ceramic balls arranged alternately in rows and columns, as shown in Fig. 1. In the triple-diameter configuration, the layers of large, medium, and small balls each constitute 1/3 of the total thickness. In the double-diameter configuration, the large-diameter ceramic ball layer constitutes 3/5 of the total thickness, while the small-diameter layer constitutes 2/5, as shown in Fig. 2. The ceramic balls were homogeneously distributed in the single-diameter ceramic ball combination structure (Fig. 2). The three configurations were categorized into three major types based on ceramic ball diameter combinations. Specific dimensions of the protective structures and ceramic ball diameters are summarized in Table 1.

Owing to the geometric symmetry of the target plate of the ceramic ball/nylon elastomer composite, a 1/2 model was adopted to better observe the response of the projectile penetrating through the protective structure and to improve the computational efficiency. In the ANSYS/LS-DYNA finite element software, SOLID168 solid elements were used for modeling, and the model was meshed with hexahedral elements. The interlayer interfaces (steel-nylon, ceramic-nylon) were simulated using the *CONTACT_AUTOMATIC_SURFACE_TO_ SURFACE_TIEBREAK

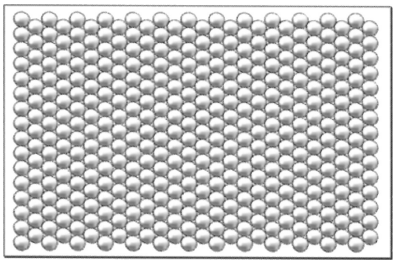

Fig. 1. Ceramic ball single-layer layout.

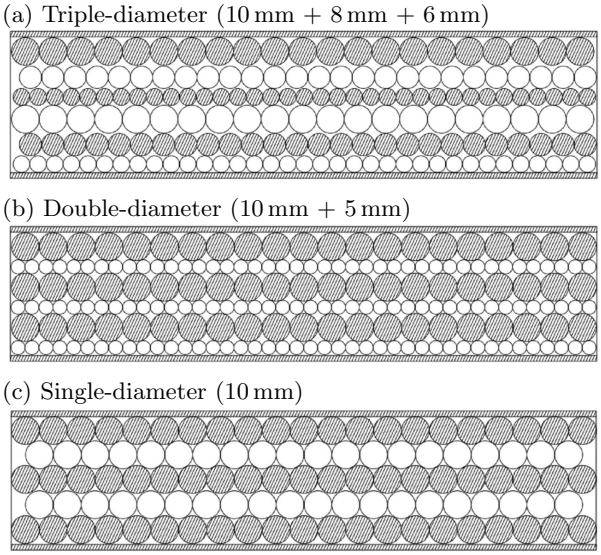

Fig. 2. Sectional view of ceramic ball/nylon elastomer composite structure.

Table 1. Ceramic ball diameter and arrangement in protective panels.

Target number	Single-diameter	Target number	Double-diameter		Target number	Triple-diameter		
	Ball diameter [mm]		Ball 1 diameter [mm]	Ball 2 diameter [mm]		Ball 1 diameter [mm]	Ball 2 diameter [mm]	Ball 3 diameter [mm]
S1	5	D1	5	2.5	T1	8	6	4
S2	6	D2	6	3	T2	9	7	5
S3	7	D3	7	3.5	T3	10	8	6
S4	8	D4	8	4	T4	11	9	7
S5	9	D5	9	4.5	T5	12	10	8
S6	10	D6	10	5	T6	13	11	9
S7	11	D7	11	5.5	T7	14	12	10
S8	12	D8	12	6	T8	15	13	11
S9	13	D9	13	6.5	T9	16	14	12
S10	14	D10	14	7				
S11	15	D11	15	7.5				
S12	16	D12	16	8				

contact algorithm to characterize the interfacial bond failure behavior. In the penetration simulations, both round-nose and flat-nose projectiles were used (diameter: 8.08 mm, mass: 8 g). The round-nose projectiles had a length of 21.34 mm, while the flat-nose projectiles had a length of 20 mm. The projectile model is shown in Fig. 3, and the target plate model is shown in Fig. 4.

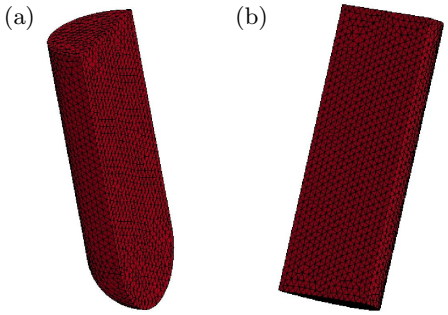

Fig. 3. Numerical model of a half-projectile: (a) round-nose bullet; (b) flat-nose bullet.

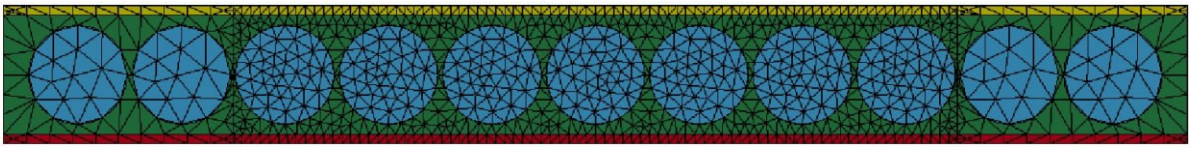

Fig. 4. Example of the target plate model for protective structure (single-layer structure).

2.2. Material constitutive model and parameters

The material of the projectile body (round-nose and flat-nose) is tool steel; Q235 steel is used for the front and back steel plates of the protective structure, and the Johnson–Cook constitutive model was adopted for the numerical simulations of these two materials, as shown:

$$\sigma_y = \left(A + B\overline{\varepsilon}_p^n\right)\left(1 + c\ln\overline{\varepsilon}^*\right)\left[1 - \left(\frac{T - T_r}{T_m - T_r}\right)^m\right]. \tag{2.1}$$

The model can describe the large deformation and high strain rate characteristics of metal materials, with the relevant parameters listed in Table 2 and Table 3.

Table 2. Johnson–Cook constitutive model parameters of the projectile body.

ρ [kg · m^{-3}]	G [MPa]	T_r [K]	T_m [K]	A [MPa]	B [MPa]	n	C	m	$\dot{\varepsilon}_0$	d_1	d_2
7830	770	293	1795	792.0	510.0	0.26	0.0640	1.03	0.1×10^{-5}	0	0.4

Table 3. Johnson–Cook constitutive model parameters for Q235 steel.

ρ [kg · m^{-3}]	G [MPa]	T_r [K]	T_m [K]	A [MPa]	B [MPa]	n	C	m	$\dot{\varepsilon}_0$	d_1	d_2
7800	798	293	1795	240.0	230.2	0.578	0.0652	0.706	2.1×10^{-3}	−0.0193	3.811

The material grade of the nylon elastomer is polyamide-6, and its constitutive relationship is described by the Cowper–Symonds model with the equation:

$$\sigma_Y = \left[1 + \left(\frac{\dot{\varepsilon}}{C}\right)^{1/P}\right]\left(\sigma_0 + \beta E_p \varepsilon_p^{\text{eff}}\right), \tag{2.2}$$

where σ_0 is the initial yield stress, $\dot{\varepsilon}$ is the strain rate, C and P are the strain rate parameters, $\varepsilon_p^{\text{eff}}$ is the effective plastic strain, and E_p is the plastic hardening modulus. The relevant material parameters of the nylon elastomer are shown in Table 4.

The ceramic ball is made of Al_2O_3, and the JOHNSON_HOLMQUIST_CERAMICS model, also known as the JH model, is selected for numerical simulation. The damage model consisting of strength and cumulative damage failure is particularly suitable for describing the damage mode of brittle materials such as ceramics and glass.

Table 4. Parameters of the Cowper–Symonds constitutive model for nylon elastomer.

Material	ρ [kg^{-3}]	Elastic modulus [GPa]	P	C	Poisson's ratio	$R_{P0.2}$ [Mpa]	Shear modulus [GPa]	Fracture strain
PA6	1140	3.3	0.574	1285.3	0.41	60	1.275	0.6

The equivalent stress for ceramic materials is expressed as:

$$\sigma^* = \sigma_i^* - D\left(\sigma_i^* - \sigma_f^*\right), \tag{2.3}$$

$$\sigma_i^* = a\left(p^* + t^*\right)^n \left(1 + c\ln\dot{\varepsilon}^*\right), \tag{2.4}$$

$$\sigma_f^* = b\left(p^*\right)^m \left(1 + c\ln\dot{\varepsilon}^*\right) \leq \text{SFMAX}, \tag{2.5}$$

where "*" indicates that the parameter is a dimensionless parameter, the stress is normalized by the Hugoniot elastic limit (HEL) stress. σ_i^* represents the dimensionless equivalent stress when the material is intact, σ_f^* represents the dimensionless equivalent stress when the material is damaged. D represents the damage factor of ceramic, which ranges from 0 to 1; $D = 0$ corresponds to the intact state, and $D = 1$ represents complete material failure. The pressure is normalized by the hydrostatic pressure p_{HEL} at the HEL, $p^* = p/p_{\text{HEL}}$ denotes the dimensionless pressure, t^* denotes the maximum tensile hydrostatic pressure that the material can withstand, $\dot{\varepsilon}^*$ represents the dimensionless strain rate; a, c, n, b, m denote material constants. The specific material parameters are shown in Table 5.

Table 5. JH constitutive model parameters of ceramic balls.

G [GPa]	ρ [g · cm^{-3}]	σ_{HEL} [GPa]	a	n	c	b	m	$\dot{\varepsilon}_0$
90.16	3.7	6.7	0.88	0.64	0.003	0.28	0.6	1×10^{-6}
PHEL [GPa]	BULK	k_1	k_2	k_3	d_1	d_2	SFMAX	
3.63	1	130.95	0	0	0.005	0.7	1.6	

Equation (2.6) defines the damage as the accumulated ratio of incremental plastic strain to the corresponding critical fracture strain at each step, which can reflect the evolution process of the initiation and gradual propagation of microcracks and microdefects inside the material with plastic deformation. The ceramic damage factor is expressed by:

$$D = \sum \frac{\Delta\varepsilon^p}{\varepsilon_f^p} = \sum \frac{\Delta\varepsilon^p}{d_1\left(p^* + f_t^*\right)^{d_2}}, \tag{2.6}$$

where $\Delta\varepsilon^p$ is the increase in plastic strain at each incremental step, ε_f^p is the plastic fracture strain, and d_1, d_2 are damage constants.

The ceramic ball is not fully damaged; its material equation of state is expressed by:

$$p = k_1\mu + k_2\mu^2 + k_3\mu^3, \tag{2.7}$$

where k_1, k_2, k_3 are constants, $u = \frac{p}{p_0} - 1$, ρ_0 is the initial density, and ρ is the present density.

2.3. Experimental validation of the numerical simulation method for penetration

To validate the numerical simulation methodology, an experiment consistent with the numerical simulation model was conducted, and the numerical simulation results were compared with real ballistic test data. Specifically, the experiment was performed using a standard single-stage light gas gun. First, 8.08 mm-diameter round-nose or flat-nose projectiles were mounted

in a sabot, and loaded into the gun barrel. High-pressure gas accelerates the sabot and embedded projectile, which then penetrates the target plate after passing through the sabot separator, as shown in Fig. 5.

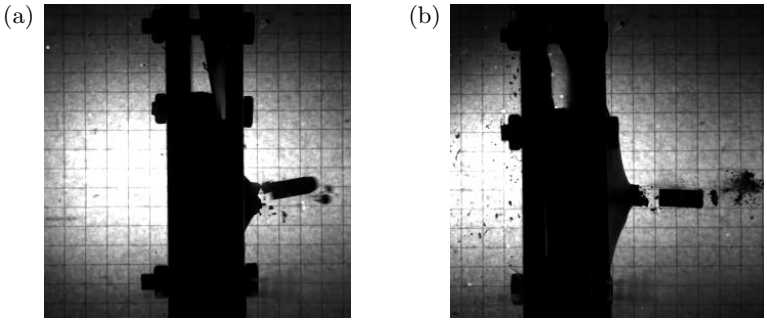

Fig. 5. Penetration of the projectile into the ceramic composite target plate: (a) round-nose bullet; (b) flat-nose bullet.

The protective structure was bolted to the target chamber, with front and rear steel plates each having dimensions of 200 mm × 200 mm × 0.5 mm. The central nylon-ceramic ball composite layer had a cross-sectional size of 130 mm × 130 mm. Three sets of test specimens were prepared for the target plate: a single layer of 5 mm diameter ceramic balls, a single layer of 10 mm diameter ceramic balls, and a double layer (5 mm + 10 mm diameter ceramic balls), as shown in Fig. 6. Detailed parameters of the target plate are provided in Table 6.

(a) A layer of 5 mm diameter ceramic ball protective structure

(b) A layer of 10 mm diameter ceramic ball protective structure

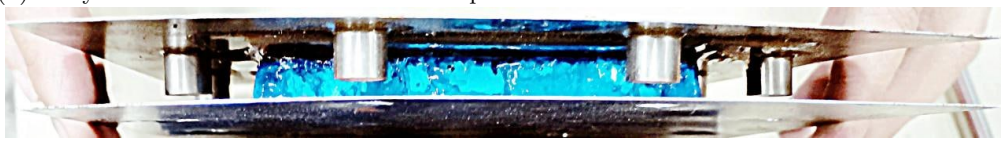

(c) Two layers (10 mm + 5 mm) diameter ceramic ball protective structure

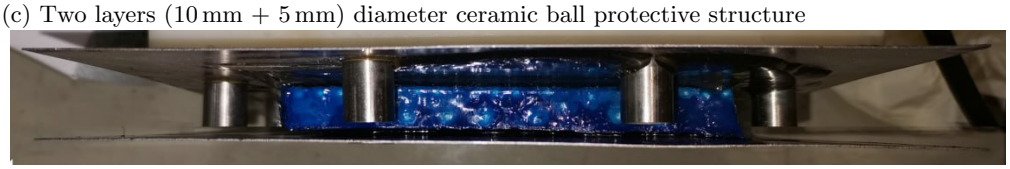

Fig. 6. Three prepared ceramic ball/nylon elastomer composite protective structures.

Table 6. Parameters of ceramic ball/nylon elastic composite structure target plate.

Bullet category	Target plate number	Target board size [mm]	Ceramic ball layers	Ceramic ball diameter [mm]
Round-nose bullet	SDY	200 × 200	1	5
	DDY		1	10
	SY		2	First floor: 5, second floor: 10
Flat-nose bullet	SDP	200 × 200	1	5
	DDP		1	10
	SP		2	First floor: 5, second floor: 10

As shown in Table 7, the relative errors between the experimental and numerical simulation data are generally within 10 % in the residual velocity under identical test conditions, with a few outliers (e.g., DDP-1, DDP-2), indicating that the numerical simulation has good reliability. The relative errors between the numerical simulation data and the experimental data are in the range of 12 % to 18 %, which is within acceptable limits.

Table 7. Comparison of experimental and simulation data for the ceramic ball protection structure.

Target number	Experimental data			Simulation data		Residual velocity error [%]	Deviation angle error [%]
	Initial speed [m/s]	Residual velocity [m/s]	Bullet deflection [°]	Residual velocity [m/s]	Bullet deflection [°]		
SDY-1	306.37	104.91	14.69	115.16	17.41	9.77	18.52
SDY-2	299.15	123.16	8.8	110.05	10.10	10.64	14.77
SDP-1	289.35	158.73	2.3	176.54	2.69	11.22	16.96
SDP-2	287.46	162.46	4.96	175.31	5.57	7.91	12.30
DDY-1	291.35	5.91	11.45	6.51	13.51	10.15	17.99
DDY-2	295.03	21.08	11.84	7.64	13.72	63.76	15.88
DDP-1	273.14	No breakdown	/	16.55	10.14	/	/
DDP-2	278.81	No breakdown	/	18.03	9.35	/	/
SY-1	288.27	No breakdown	/	No breakdown	/	/	/
SY-2	293.14	No breakdown	/	No breakdown	/	/	/
SP-1	304.48	No breakdown	/	No breakdown	/	/	/
SP-2	295.03	No breakdown	/	No breakdown	/	/	/

Good agreement between experimental and numerical results was observed for most specimen groups, except for DDP-1 and DDP-2. In these cases, the numerical simulation predicted complete penetration (residual velocity > 0 m/s), whereas no penetration was observed in the experiment (residual velocity $= 0$ m/s). This discrepancy can be attributed to the uncertainties in the experiments, including differences in homogeneity and compactness of the ceramic spheres encapsulated in the nylon matrix, as well as the deviation in the actual position of the projectile's impact point. These factors lead to the fluctuation of the experimental results. However, the overall numerical simulation errors for the residual velocity and the projectile's deflection angle remain within a reasonable range.

Figure 7 shows the rupture morphology of round-nose and flat-nose projectiles following penetration of the ceramic composite protective structure, under both numerical simulation and experimental conditions. Moreover, the breach morphologies from the simulation and the experiment are in close agreement. Regardless of the projectile shape, the breach exhibits a petal-like shape; notably, the breach formed by the flat-nose projectile is larger than that formed by the round-nose projectile.

For the SY-1, SY-2, SP-1, and SP-2 ceramic composite protective structures – which remained unpenetrated in experiments – the numerical simulations also consistently showed no penetration. As shown in Fig. 8, both simulation and experimental results exhibit pronounced bulging deformation on the rear surface of the protective structure. The deformation modes and bulge dimensions are in close agreement, with a bulge deformation of approximately 8 mm observed in both cases.

In summary, the validity of the material model parameters and ANSYS/LS-DYNA finite element model setup was verified by comparing the numerical simulation results of the penetration process with the experimental results, demonstrating the accuracy of the established numerical simulation method.

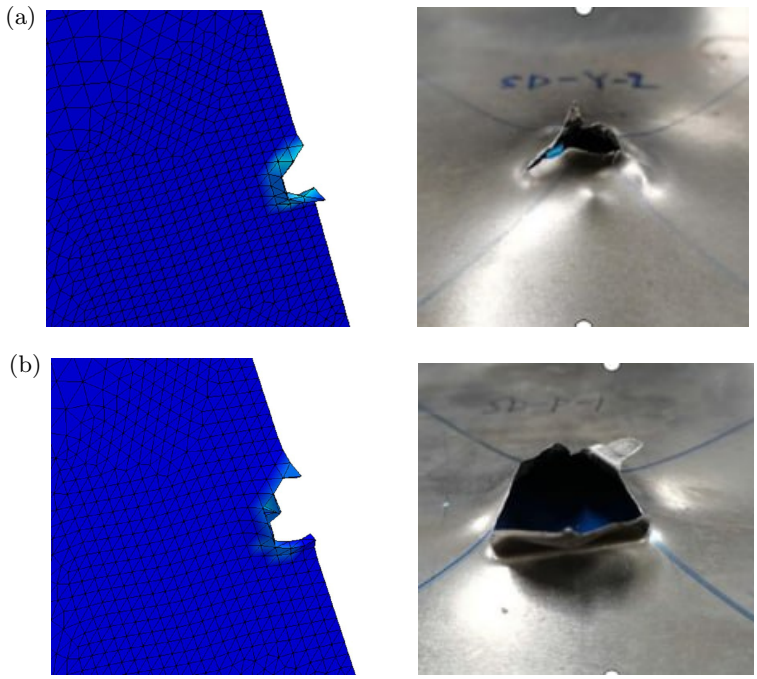

Fig. 7. Comparison between simulated and experimental results for the breach of the protective structure: (a) round-nose bullet; (b) flat-nose bullet.

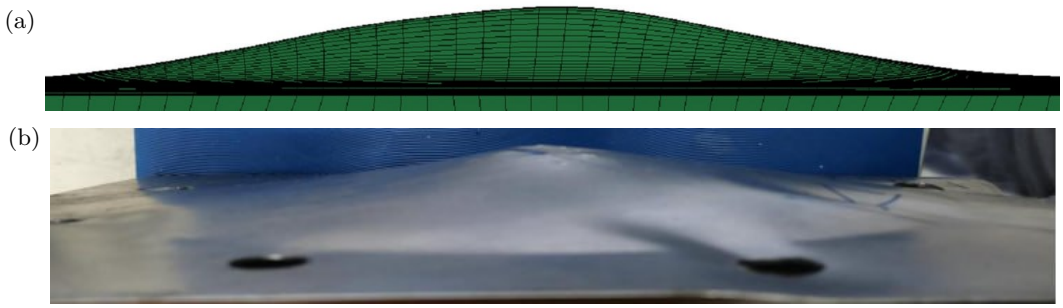

Fig. 8. Comparison between simulated and experimental results for the protrusion of the structure: (a) simulation diagram; (b) experimental diagram.

3. Influence of ceramic ball diameter combinations on the penetration resistance of protective structures

3.1. Comparison and analysis of the penetration resistance of ceramic ball protective structures with different ceramic ball diameter combinations

To more directly and clearly understand the residual velocities of various ceramic composite protective structures under projectile penetration, the residual velocities of round-nose and flat-nose projectiles at an impact velocity of 600 m/s are plotted in line charts. For simplicity and clarity of the charts, the x-axis is labeled with the diameter of the first row of ceramic balls behind the impact face of the protective structure, as shown in Fig. 9 and Fig. 10.

As shown in the figures, the residual velocities of all protective structures against both bullets exhibit a V-shaped pattern of decreasing and then increasing under an initial impact velocity of 600 m/s. However, the bottom of the V-shaped curve for the double-diameter ceramic ball protective structure is flatter and the velocity change is more gradual. Furthermore, among the three types of composite protective structures, when the diameter of the first layer of ceramic balls is the same, the residual velocity of the projectile for the double-diameter composite protective structure is lower.

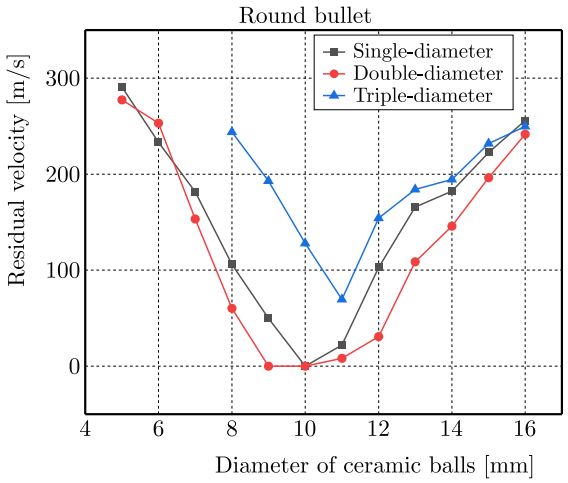

Fig. 9. Residual velocity of protective structure under the impact of round-nose projectile.

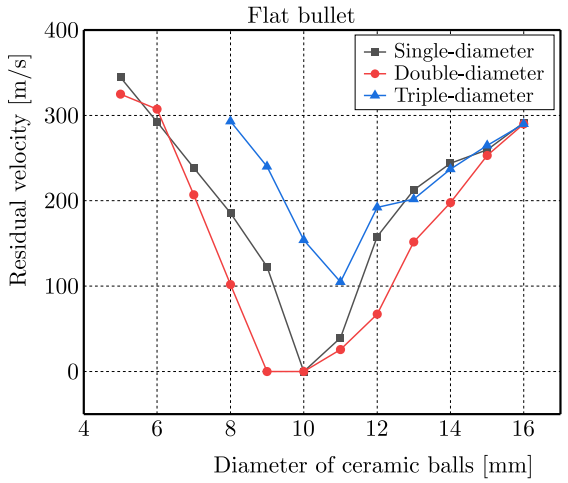

Fig. 10. Residual velocity of the protective structure under the impact of a flat-nose projectile.

Among them, two sets of zero residual velocities were observed for the double-diameter ceramic ball protective structure for both projectile shapes, one set was observed for the single-diameter structure, and none of the zero values were observed for the triple-diameter structure. Overall, the average residual velocity of the double-diameter structure is 33.4 m/s lower than that of the single-diameter structure, while the residual velocity of the triple-diameter structure is 97.1 m/s higher than that of the double-diameter structure. These results indicate that the three structures are ranked by penetration resistance as follows: double-diameter ceramic ball protective structure > single-diameter ceramic ball protective structure > triple-diameter ceramic ball protective structure.

Under penetration by both round-nose and flat-nose projectiles, the double-diameter ceramic ball composite protective structure exhibits significantly superior penetration resistance compared to the triple-diameter and single-diameter ceramic ball composite structures. This advantage can be attributed to two mechanisms: (1) the relatively larger ceramic balls in the double-diameter structure effectively degrade the projectile's kinetic energy by consuming it, abrading the projectile's surface, and inducing yaw; (2) as the impact force is transmitted from the frontal ceramic balls to the internal structure, the region composed of smaller ceramic balls and the nylon matrix rapidly distributes the load, thereby activating more ceramic balls and the matrix material in a collective resistance against penetration.

In contrast, the single-diameter ceramic ball composite structure engages a relatively limited number of ceramic balls and nylon matrix during impact. For the triple-diameter ceramic ball

composite structure, the proportion of nylon matrix dedicated to dissipating the projectile's kinetic energy is insufficient during penetration.

The double-diameter structure, however, achieves an optimal balance between energy dissipation and collaborative protection by rationally matching the proportions of ceramic balls to the nylon matrix, thereby producing the optimal protective effect.

3.2. Effect of ceramic ball diameter on the penetration resistance of the protective structure

A comparison of the data in Fig. 11 to Fig. 13 indicates that, for all three types of composite protective structures, the residual velocity of the round-nose projectile is lower than that of the flat-nose projectile. This indicates that these three types of structures provide better protective effectiveness against round-nose projectiles.

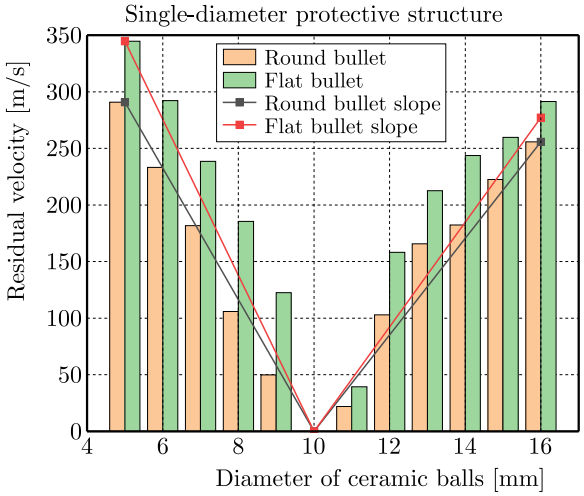

Fig. 11. Projectile residual velocity diagram for single-diameter ceramic ball composite structure.

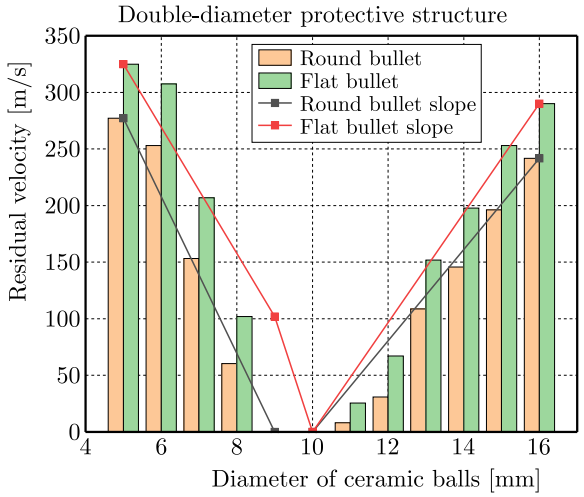

Fig. 12. Projectile residual velocity diagram for double-diameter ceramic ball composite structure.

For the single- and double-diameter ceramic ball structures: when the diameter of the front-row ceramic balls ranges from 8 mm to 11 mm, the structures generally exhibit superior penetration resistance. If the diameter is less than 8 mm or greater than 11 mm, the penetration resistance decreases significantly. Notably, when the maximum diameter of the ceramic balls is approximately 10 mm, the projectile's residual velocity drops to 0 m/s (i.e., the structure is not penetrated), achieving the optimal protective effect. For the triple-diameter ceramic ball

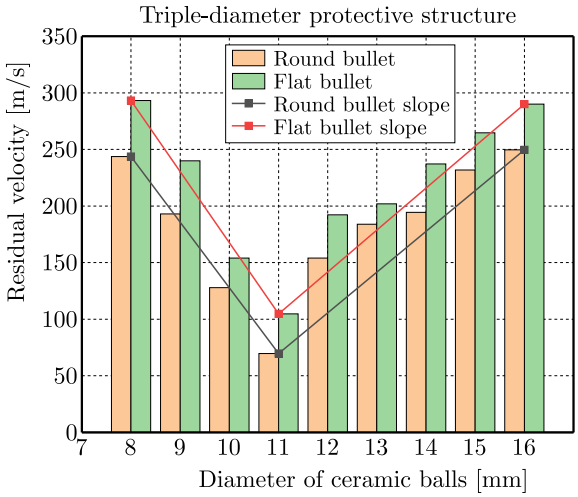

Fig. 13. Projectile residual velocity diagram for triple-diameter ceramic ball composite structure.

composite: the structure remains unpenetrated (residual velocity = 0 m/s) under all tested conditions. When the ceramic ball diameter is 11 mm, the structure exhibits the lowest residual velocity (though still non-zero).

Using the ceramic ball diameter corresponding to the minimum residual velocity (i.e., the critical diameter) as a reference, the slope of the ceramic ball diameter-residual velocity curve indicates that: below the critical diameter, the residual velocity decreases as the ball diameter increases (negative slope). Above the critical diameter, the residual velocity increases as the ball diameter increases (positive slope).

For all three configurations, the absolute value of the curve slope in the region above the critical diameter is smaller than that in the region below it, indicating that increasing ceramic ball diameter has a more gradual effect on residual velocity when the diameter is larger than the critical value.

Further analysis of the double-diameter structure, which exhibits optimal performance, shows that superior penetration resistance is generally achieved when the ceramic ball diameter exceeds that of the projectile. However, if the ceramic ball diameter is much larger than the projectile diameter, the protective performance declines markedly. The optimal performance occurs when the ratio of the projectile diameter to the ceramic ball diameter falls within the range of 0.73 to 1.01 (corresponding to a ceramic ball diameter range of approximately 8 mm to 11 mm).

4. Effect of two ceramic ball diameters and their double-diameter ratio on the penetration resistance of double-diameter ceramic ball composite protective structures

4.1. Selection of ceramic ball proportion and diameter

A double-diameter ceramic ball composite protective structure with superior penetration resistance was selected for in-depth study. Given that this double-diameter ceramic ball composite protective structure exhibits optimal penetration resistance when the diameter of the front-row ceramic balls ranges from 8 mm to 11 mm, the diameters of the front-row ceramic balls in the numerical model of this section are set to 7 mm, 8 mm, 9 mm, 10 mm, 11 mm, and 12 mm. The diameter ratio of the front-row ceramic balls relative to the rear-row ceramic balls ranges from 0.8 to 3.5.

The protective structures are divided into 6 groups based on the diameter of the front-row ceramic balls. Within each group, the diameter of the rear-row ceramic balls is further subdivided

based on the diameter ratio (η) relative to that of the front-row ceramic balls. The structures are composed of intact ceramic balls, with the total thickness controlled at approximately 50 mm. Specifically: the thickness of the front-row ceramic ball region makes up about 2/3 of the total thickness, while the rear-row ceramic ball region accounts for about 1/3 of the total thickness. The specific dimensional parameters of the ceramic balls for each group are detailed in Table 8.

Table 8. Parameters of various ceramic ball composite protection structures.

Front row ball	Diameter of the ball at the back										Unit
7 mm diameter	8.8	6.4	5.0	4.1	3.5	3.0	2.7	2.4	2.2	2.0	mm
8 mm diameter	10	7.3	5.7	4.7	4.0	3.5	3.1	2.8	2.5	2.3	mm
9 mm diameter	11.3	8.2	6.4	5.3	4.5	3.9	3.5	3.1	2.8	2.6	mm
10 mm diameter	12.5	9.1	7.1	5.9	5.0	4.3	3.8	3.4	3.1	2.9	mm
11 mm diameter	13.8	10	7.9	6.5	5.5	4.8	4.2	3.8	3.4	3.1	mm
12 mm diameter	15	10.9	8.6	7.1	6.0	5.2	4.6	4.1	3.9	3.4	mm
Ball diameter ratio	0.8	1.1	1.4	1.7	2.0	2.3	2.6	2.9	3.2	3.5	η

4.2. Analysis of the effect of ceramic ball diameter and ceramic ball diameter ratio on the projectile's residual velocity

Round-nose and flat-nose projectiles penetrated the ceramic ball composite protective structures at an impact velocity of 600 m/s. The residual velocities of the projectiles after penetrating the double-diameter ceramic ball structures with different diameter ratios were obtained, as shown in Fig. 14.

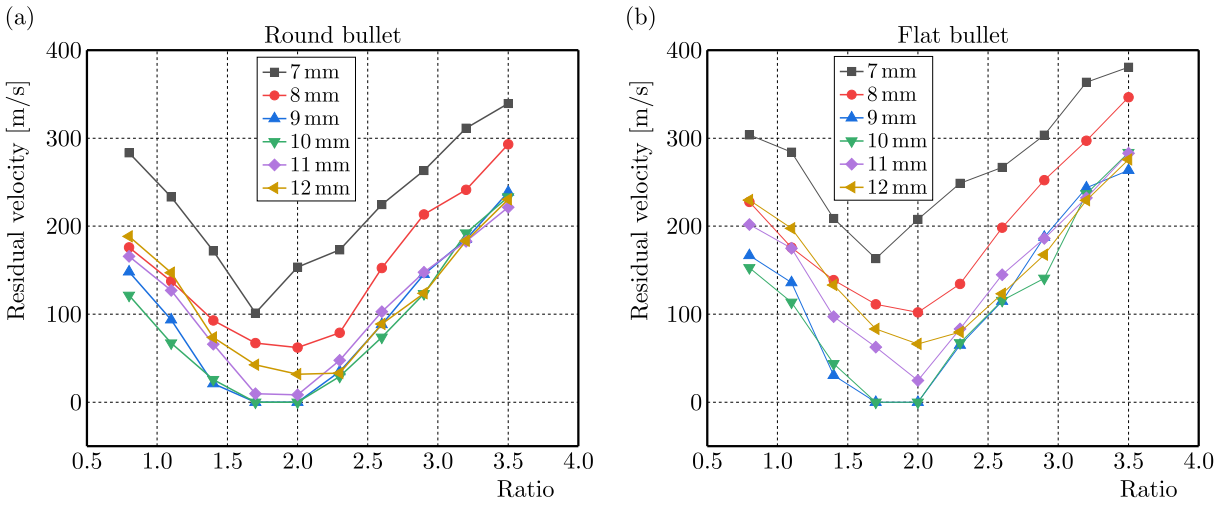

Fig. 14. Residual velocity of the ceramic ball protective structure for the same projectile: (a) round-nose bullet; (b) flat-nose bullet.

Figure 14 indicates that when the round-nose and flat-nose projectiles penetrate the ceramic ball protective structure with different ceramic ball diameter ratios, the residual velocities of both round-nose and flat-nose projectiles exhibit a V-shaped trend, characterized by an initial decrease followed by an increase. However, the bottom of the V-shaped curve for the round-nose projectiles is flatter, indicating a more gradual velocity transition. The data reveal that the residual velocity of the round-nose projectile is lower than that of the flat-nose projectile. This demonstrates that the double-diameter ceramic ball protective structure is more effective against round-nose projectiles, which is consistent with the previous conclusion.

The data indicate that residual velocity decreases gradually until reaching the optimal diameter ratio threshold (about 2.0), beyond which it rises steeply. For instance, when a round-nose projectile penetrates a protective structure fronted with 8 mm ceramic balls, the residual velocity rapidly increases as the ceramic ball diameter ratio rises to 2.6, reaching a level equivalent to that observed at a ratio of 0.8. This demonstrates that exceeding the optimal diameter ratio significantly degrades protective performance, leading to a sharp decline in anti-penetration capability.

The analyses indicate that, for both round-nose and flat-nose projectiles, the residual velocity of the projectiles exhibits a decreasing-then-increasing trend as the diameter of the front-row ceramic balls ranges from 7 mm to 12 mm. This confirms the significant influence of the ceramic ball diameter ratio on the penetration resistance of the composite protective structure.

Within the specific diameter ratio range of 1.7–2.0, the fluctuation in the residual velocity of round-nose projectiles narrows considerably (average fluctuation range: 32.9 m/s). This demonstrates that a ceramic ball size gradient (i.e., diameter ratio) within this range effectively optimizes the penetration resistance of the structure. For flat-nose projectiles, the magnitude of residual velocity change (52.7 m/s) over the same diameter ratio interval (1.7–2.0) is larger than for round-nose projectiles. Nevertheless, this change remains relatively small compared to the overall variation range, indicating that the ceramic ball composite protective structure maintains stable and effective penetration resistance within this specific diameter ratio range.

When the front-row ceramic balls have a diameter of 9 mm or 10 mm, the residual velocities of the projectiles across various diameter ratios are significantly lower. This indicates enhanced penetration resistance of the double-diameter ceramic ball composite protective structure. Notably, within the diameter ratio range of 1.7 to 2.0, the residual velocities of both round-nose and flat-nose projectiles drop to zero (i.e., the structure remains unpenetrated), thus yielding optimal protective effectiveness.

Based on the above analysis, the protective structure achieves optimal penetration resistance when the ceramic ball diameter ratio falls within the range of 1.7 to 2.0. On the one hand, if the ratio is too small, the rear-row ceramic balls become excessively large. This results in an insufficient number of rear-row ceramic balls participating in load transfer when the projectile's impact load propagates from front to rear, thereby compromising the structure's overall anti-penetration capacity. On the other hand, if the ratio is too large, the rear-row ceramic balls become excessively small. Although this increases the number of ceramic balls involved in load transfer, the inadequate compressive strength of smaller ceramic balls likewise fails to enhance the structure's penetration resistance.

5. Conclusion

This study designed ceramic ball/nylon elastomer composite structures with different ceramic ball diameters and arrangement modes, and conducted penetration tests on target plates with different structural forms using 8.08 mm round-nose/flat-nose projectiles. Combined with numerical simulations, the following main conclusions were obtained:

1) For both round-nose and flat-nose projectiles, the double-diameter ceramic ball protective structure outperforms the single-diameter and triple-diameter structures in penetration resistance. Additionally, all three types of protective structures (single-diameter, double-diameter, and triple-diameter) exhibit superior resistance to round-nose projectiles compared to flat-nose projectiles.
2) When 8.08 mm-diameter round-nose and flat-nose projectiles penetrate the double-diameter ceramic ball protective structure, penetration resistance improves with ceramic balls larger than the projectile diameter. However, protective efficacy deteriorates markedly when the ball diameter exceeds the projectile diameter by over 4 mm. Optimal anti-penetration performance occurs within the 0.73–1.01 projectile-to-ceramic-ball diameter ratio range for

the first-row ceramic balls immediately behind the strike-face, corresponding to strike-face ceramic ball diameters of 8 mm to 11 mm.

3) In the double-diameter ceramic ball protective structure, the residual velocity drops to zero when the front-to-rear ceramic ball diameter ratio is 1.7–2.0 (front-row ceramic ball diameter: 9 mm to 10 mm), resulting in complete protection (i.e., the structure remains unpenetrated).

References

1. Aktaş, L.T., & Çevik, M. (2025). Ballistic impact analysis of composite armors incorporating prismatic and spherical self-healing ceramic structures. *Mechanics of Composite Materials*, *61*(4), 739–752. https://doi.org/10.1007/s11029-025-10306-6
2. Andraskar, N., Tiwari, G., Goel, M.D., & Senthil, K. (2023). Numerical investigation of the effect of layering thickness on the ballistic response of ceramic/metal composite structure. *Mechanics of Solids*, *58*(4), 1351–1369. https://doi.org/10.3103/S002565442360071X
3. Beissel, S.R., & Johnson, G.R. (2000). An abrasion algorithm for projectile mass loss during penetration. *International Journal of Impact Engineering*, *24*(2), 103–116. https://doi.org/10.1016/S0734-743X(99)00146-3
4. Cao, J., Lai, J., Zhou, J., Kang, N., Du, L., & Miao, Y. (2020). Experiments and simulations of the ballistic response of ceramic composite armors. *Journal of Mechanical Science and Technology*, *34*(7), 2783–2793. https://doi.org/10.1007/s12206-020-0611-8
5. Fawaz, Z., Zheng, W., & Behdinan, K. (2004). Numerical simulation of normal and oblique ballistic impact on ceramic composite armours. *Composite Structures*, *63*(3–4), 387–395. https://doi.org/10.1016/S0263-8223(03)00187-9
6. Feli, S., & Asgari, M.R. (2011). Finite element simulation of ceramic/composite armor under ballistic impact. *Composites Part B: Engineering*, *42*(4), 771–780. https://doi.org/10.1016/j.compositesb.2011.01.024
7. Feng, X., & Zhu, P. (2024). Study of impact resistance of a novel bio-inspired ceramic-composite structure using finite element simulations. *Mechanics of Advanced Materials and Structures*, *31*(25), 7420–7433. https://doi.org/10.1080/15376494.2023.2245813
8. Lee, M., & Yoo, Y.H. (2001). Analysis of ceramic/metal armour systems. *International Journal of Impact Engineering*, *25*(9), 819–829. https://doi.org/10.1016/S0734-743X(01)00025-2
9. Schwer, L.E., & Day, J. (1991). Computational techniques for penetration of concrete and steel targets by oblique impact of deformable projectiles. *Nuclear Engineering and Design*, *125*(2), 215–238. https://doi.org/10.1016/0029-5493(91)90079-W
10. Tan, K., Shen, C., Chen, H., Wang, J., Cai, C., Zhang, H., & Liu, C. (2021). *Composite protection plate with non-equal-diameter ceramic balls* (Patent No. CN 212409494 U). https://patents.google.com/patent/CN212409494U/en?oq=CN+212409494+U+2011+
11. Tan, M., Zhang, X., Xiong, W., Liu, C., Han, G., & Li, Y. (2023). Influence of layered back plate on the ballistic performance of ceramic armor. *Composite Structures, 308*, Article 116688. https://doi.org/10.1016/j.compstruct.2023.116688
12. Woodward, R.L. (1990). A simple one-dimensional approach to modelling ceramic composite armour defeat. *International Journal of Impact Engineering*, *9*(4), 455–474. https://doi.org/10.1016/0734-743X(90)90035-T
13. Zaera, R., Sánchez-Sáez, S., Pérez-Castellanos, J.L., & Navarro, C. (2000). Modelling of the adhesive layer in mixed ceramic/metal armours subjected to impact. *Composites Part A: Applied Science and Manufacturing*, *31*(8), 823–833. https://doi.org/10.1016/S1359-835X(00)00027-0

Manuscript received October 28, 2025; accepted for publication February 18, 2026; published online April 21, 2026.